Air Cooling Concepts for Li-Ion Battery Pack in Cell Level

Conference Paper · July 2017

DOI: 10.1115/HT2017-4701

4 authors, including:

Kuo-Huey Chen
General Motors Company
76 PUBLICATIONS **762** CITATIONS
SEE PROFILE

Taeyoung Han
General Motors Company
67 PUBLICATIONS **1,753** CITATIONS
SEE PROFILE

Bahram Khalighi
General Motors Company
81 PUBLICATIONS **990** CITATIONS
SEE PROFILE

ASME 2017 SHTC
Summer Heat Transfer Conference
July 9-14, 2017, Bellevue, WA, USA

HT2017-4701

AIR COOLING CONCEPTS FOR LI-ION BATTERY PACK IN CELL LEVEL

Kuo-Huey Chen
GM Global R&D Center
Warren, MI, USA

Taeyoung Han
GM Global R&D Center
Warren, MI, USA

Bahram Khalighi
GM Global R&D Center
Warren, MI, USA

Philip Klaus
GM Europe
Ruesselsheim, Germany

ABSTRACT

Computational Fluid Dynamics (CFD) modeling is used to study different cooling architectures for the next generation (Gen-2) EREV Li-Ion battery package. There might be advantages of air cooled batteries with respect to complexity, cost and reliability compared to liquid cooled systems like the EREV (Extended Range Electric Vehicle) GEN1 battery. Therefore, the feasibility of air cooling architectures is investigated first and later liquid cooling strategies. In this study, the thermal performance and pressure drop of the cell level for two of the core product designs are reported. The parameters considered in this study include two different heat generations (heat sources) by the battery pack and three cooling flow rates. The heat generations used are 500 *W* and 1500 *W* representing the normal driving and peak load conditions, respectively. The cooling flow rates are 100, 200 and 600 m^3/h. The battery cell temperatures, both in terms of absolute value and the variation within the cell, and the pressure drop which is related to the required pumping power, are evaluated and presented.

INTRODUCTION

The Li-ion battery operation life is strongly dependent on the operating temperature and the temperature variations within each individual cell. The temperature of the cell is a direct result of the heat generation within the cell during charging and discharging states and various cooling concepts. The heat generation is due to the chemical reaction and the internal resistance within each battery cell. The amount of heat and the distribution of the heat source within the cell vary from manufacturer to manufacturer. It is, also, affected by the materials used for the reaction layers, such as polymers, metals, anode and cathode. The heat generated from the operation of the battery has to be removed efficiently and effectively to maintain the operating temperature within the limits and in rare occasions to prevent a thermal runaway which is a condition of uncontrolled temperature rise.

The cooling strategy of the battery pack utilizing liquid as the cooling agent is very effective in removing large amount of heat with a relatively low flow rate. However, the liquid cooling system requires more careful attention such as leakages and corrosions. It also costs more to operate and carries more weight. On the other hand, air cooling is believed to be much simpler, lighter and easier to maintain. However, air has much smaller heat capacity than liquid and, thus, a much higher volumetric flow rate is required to achieve the same cooling performance. Packaging is also a challenging issue. An air cooled battery needs larger manifolds for air supply. That leads to larger overall package compared to the liquid cooled battery system. Another issue associated with air cooling is the noise due to moving a higher volume of air in the system.

Using CFD to conduct preliminary studies to gain insight of the cooling effectiveness for the battery cell and pack has become very attractive in terms of quick evaluation and detailed understanding of the performance. The activities include both liquid cooling [1] and air cooling [2] concepts for PHEV (Plug-in hybrid electric vehicle) or EV (Electric vehicle). Modeling the battery thermal management system is not restricted to air or liquid cooling handling alone but also extends to understand the heat source generation within the cells [3]. Recently, optimization was applied to direct air cooling for a Li-ion

battery module for hybrid electric vehicles [4] and general cooling/heating of Li-ion battery cells [5].

In the present study, two different cooling concepts are investigated. They are referred to as "channel design" and "fin design" cooling throughout this paper. In the channel design cooling concept, the cooling air is in direct contact with the battery cell surfaces by introducing the cooling air from the manifold into the cooling channels between the battery cells. For the fin design cooling concept, the cooling air is not in direct contact with the battery cell surfaces; rather, a cooling plate with fin structures are placed between the battery cells with no air flowing between the cells.

The cooling requirements or performance setting are, to some degree, related to the battery cell type and manufacturers. One example of the battery pack in the present study is shown in Fig. 1. It consists of many battery cells arranged in an I-shape. Each battery cell is about 148.6 *mm x* 190.9 *mm x* 13.2 *mm*. There is a gap of 1.2 mm between each battery cell, which is reserved for potential air cooling. The following thermal performance requirements should be met in order to maintain the life span of the battery pack.

- Battery operating temperature: 20 ^{o}C - 35 ^{o}C
- Battery heat generation:
  - 500 *W* for normal driving
  - 1500 *W* for peak load driving
- Temperature variation within battery cells:
  - < 2 ^{o}C for 500 *W*
  - < 5 ^{o}C for 1500 *W*
- Cooling air flow rate:
  - < 200 m^3/h for 500 *W*
  - < 600 m^3/h for 1500 *W*
- Pressure losses:
  - Due to expecting high flow rates, the pressure loss has to be minimized.

COOLING CONCEPT DESCRIPTIONS

A. Pin-fin channel design

The cooling air is introduced from the manifold which flows through the gap between the two adjacent battery cells. The cooling air is in direct contact with the hot battery surfaces and, therefore, the convective heat transfer is dominant in removing heat from the hot battery surfaces. In the detailed cell level simulation, it is assumed that each and every cooling channel between the two battery cells receives the same and equally distributed amount of cooling air from the manifold. This is, of course, an ideal case and this flow rate is designated as the nominal flow rate. The nominal flow rate is used to understand the heat transfer performance in an ideal cooling condition. The deviation from this ideal cooling flow distribution depends on the particular manifold design. The effect of this deviation on the cell heat transfer will be the subject in the manifold and pack level study in a separate paper.

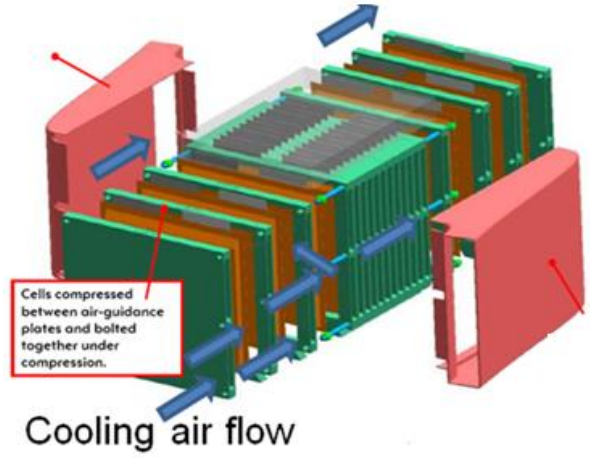

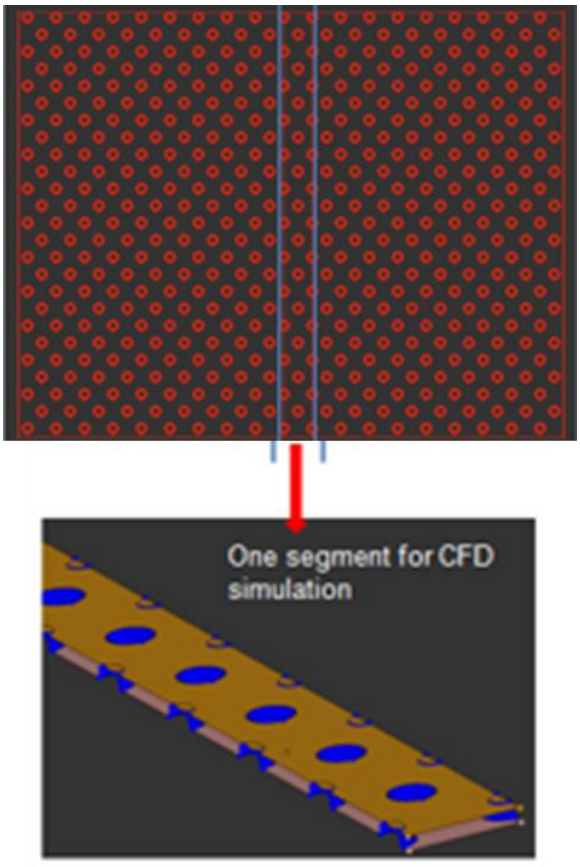

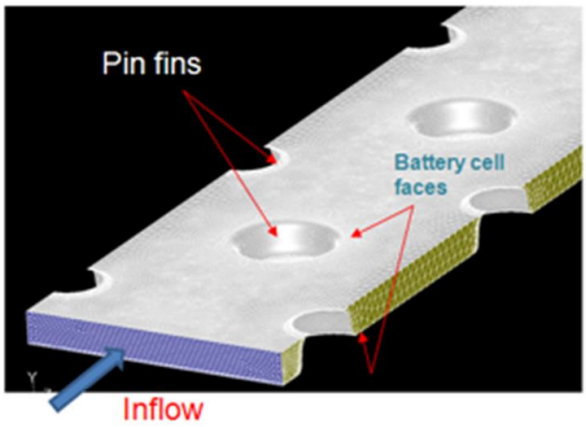

Fig. 1: Pin-fin channel structure and computational domain with a periodic segment.

Figure 1 shows the pin-fin channel structure. The channel gap between two battery cells is 1.2 *mm* and the size of the battery cell is 148.6 *mm* x 190.9 *mm*. All the simulations are performed using Fluent version 6.3.37 [6]. Three-dimensional incompressible Reynolds averaged Navier-Stokes equations with conjugate heat transfer approach are used for the simulation. The full governing equations are

$$\frac{\partial u_i}{\partial x_i} = 0 \tag{1}$$

$$\rho\left(\frac{\partial u_i}{\partial t} + u_j \frac{\partial u_i}{\partial x_j}\right) = -\frac{\partial p}{\partial x_i} + \mu\frac{\partial^2 u_i}{\partial x_j \partial x_j} + \rho g_i \tag{2}$$

$$\rho C_p\left(\frac{\partial T}{\partial t} + u_j \frac{\partial T}{\partial x_j}\right) = k\frac{\partial^2 T}{\partial x_j \partial x_j} + \dot{q} \tag{3}$$

Where, u_i is the velocity, p is the pressure, ρ is the air density, μ is the dynamic viscosity, g_i is the body force, C_p is the specific heat, k is the thermal conductivity and $\dot{q}$ is the volumetric heat generation.

As described later, the flow configurations in the present study are all in laminar regimes and no turbulence model is required. In order to take advantage of the periodic and the symmetric nature of the flow, only a portion of the battery cell is used for the computation as shown in Fig. 1. The final 3D computational domain is shown in Fig. 2. Only half thickness is used for both the upper and lower battery cells in which the symmetry condition is applied. The periodic nature of the flow in the battery width direction reduces the domain to 19 *mm* and the periodic conditions are used in the two planes. The battery walls at both the inlet and the exit locations are specified as adiabatic conditions. The total numbers of 3-D volume and 2-D surface elements are 926,489 and 2,434,196, respectively. The conditions of the heat generation in the battery cells and the air cooling flow for the study are listed as follows:

- Air cooling flow rate and temperature
  The inlet velocity for the flow rates of 100, 200 and 600 *m³/h* are 1.16, 2.33 and 6.99 *m/s*, respectively. The air inlet temperature is 303 ^0K.

- Air properties

Density (ρ), *Kg/m³:*	1.1605
Specific heat (*Cp*), *J/(kg ^0K):*	1006
Thermal conductivity (*K*), *W/(m ^0K):*	0.0263
Dynamic viscosity (*μ*), *Kg/(m s):*	1.81×10^{-5}

- Battery cell properties

Density (*ρ*):	2106
Specific heat (*Cp*):	1000
Thermal conductivity (*K*) (in-plane direction):	126
Thermal conductivity (*K*) [7]: (Cross-plane direction)	0.438

- Flow Reynolds numbers
  The Reynolds numbers for the flow rates of 100, 200 and 600 *m³/h*, based on the channel inlet velocity and channel gap of 1.2 *mm* are 89.7, 179.4 and 538.2 respectively. The cases studied in this report are all in the laminar flow regime.

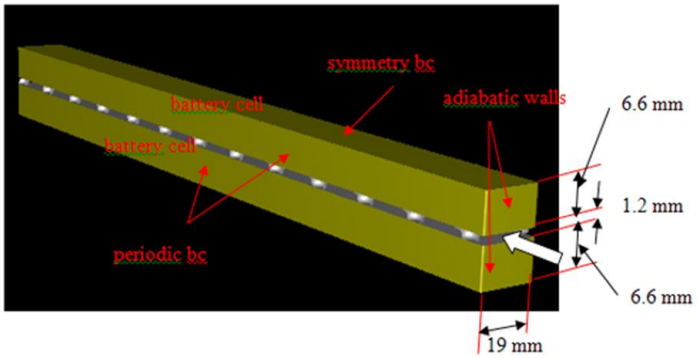

(a). Entire computational domain

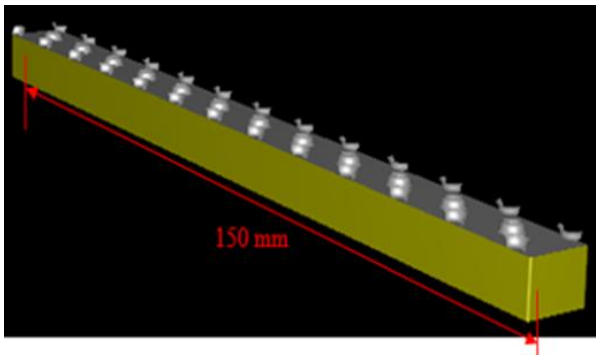

(b). Domain with upper cell removed

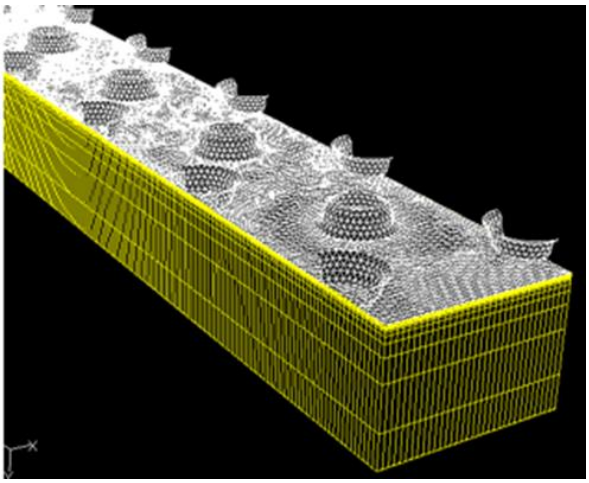

(c). Surface mesh for cell and pin-fins.

Fig. 2: (a) Entire computational domain, (b) domain with upper battery cell remove, and (c) surface mesh for battery cell and pin-fin inside the channel.

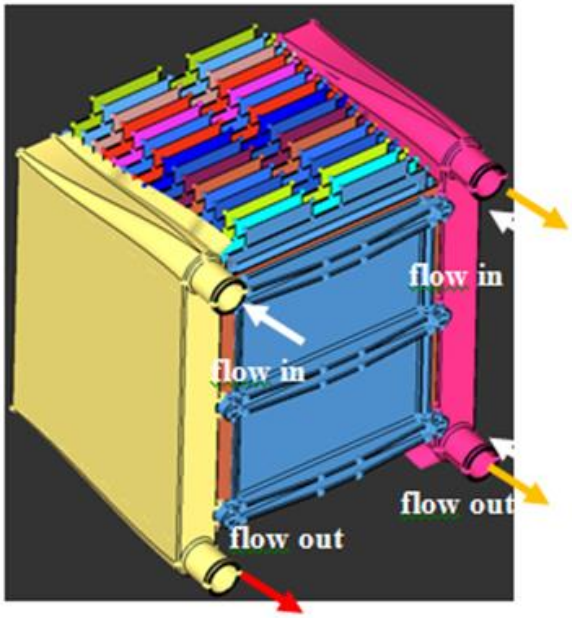

(a.) Manifold

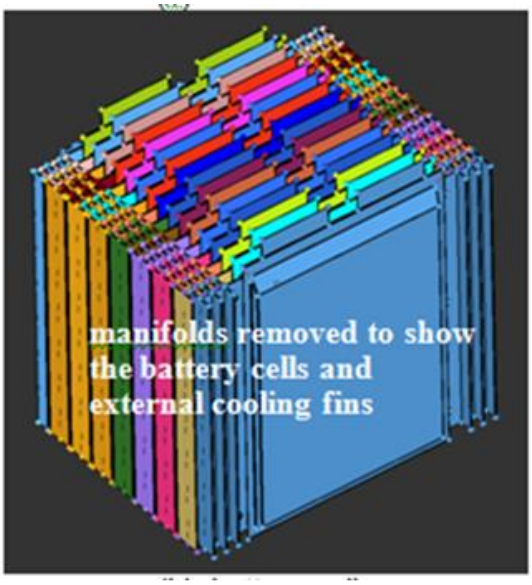

(b.) Battery cells

B. Fin outside design

In this cooling design, the cooling air is not in direct contact with the battery faces. Rather a high thermal conductivity metal plate is placed in the gap between the cells and the air cooling occurs outside the battery cells by external cooling fins connected to the cooling plates. The fin outside design cooling configuration is shown in Fig. 3.

The properties of the battery cells are identical to the one shown for the pin-fin channel cooling arrangement. However, the battery cell thickness is 10.4 *mm*, thinner than the one for the pin-fin cooling. Both the cooling plate and the attached fins are 1 *mm* thick. The cooling plates and the fins are made of aluminum. The heat generation from the battery cells and the cooling flow are the same as described for the pin-fin cooling.

The computational domain used for the analysis is again a portion of the pack due to the symmetry and periodic conditions. The computational domain is shown in Fig. 4. Due to the nature of the conjugate heat transfer cooling requirements, both the solid and fluid zones need to be meshed. The total numbers of 3-D and 2-D surface elements are 1,353,640 and 4,198,266, respectively. The inlet velocities corresponding to the flow rates of 100, 200 and 600 m^3/h cases are 0.4235, 0.847 and 2.541 *m/s*, respectively. The air inlet temperature is set to 303 ^0K. It should be noted that both co-flow and counter-flow configurations are evaluated for the fin outside design cooling.

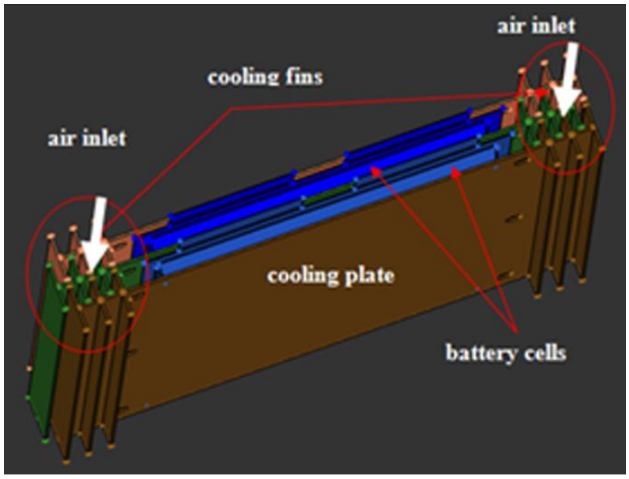

(c.) Cooling plate and the external cooling fins

Fig. 3: Fin outside design air cooling flow configuration that shows cooling plate and the external cooling fins, (a). Manifold, (b). Battery cells and (c) Cooling plate and fins.

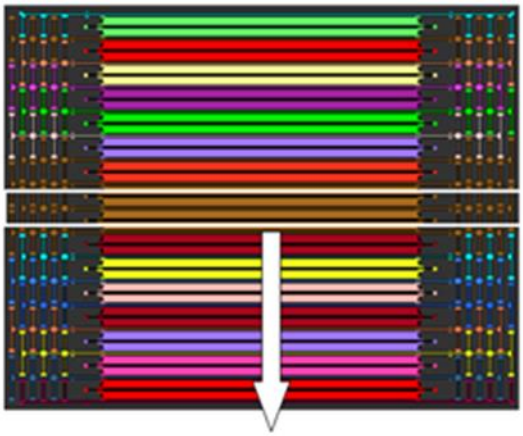

(a). Top view of the module

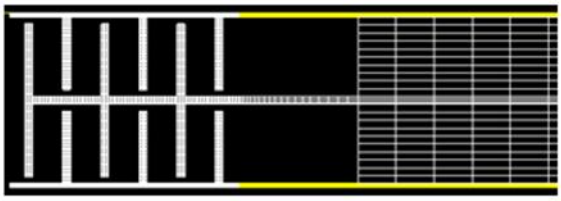

(b). Top view of the external fins

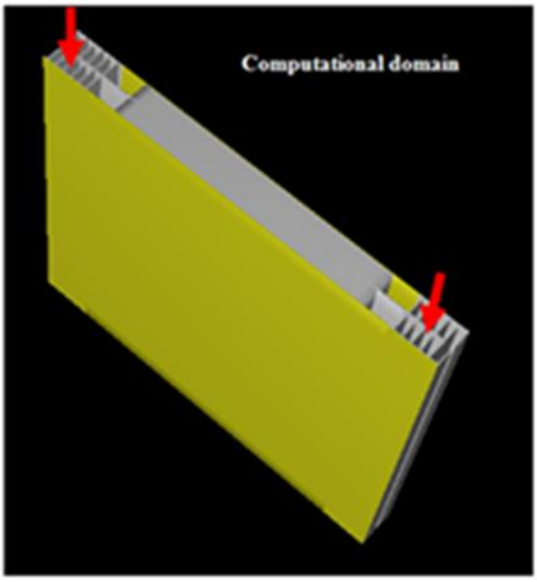

(c). Periodic sector

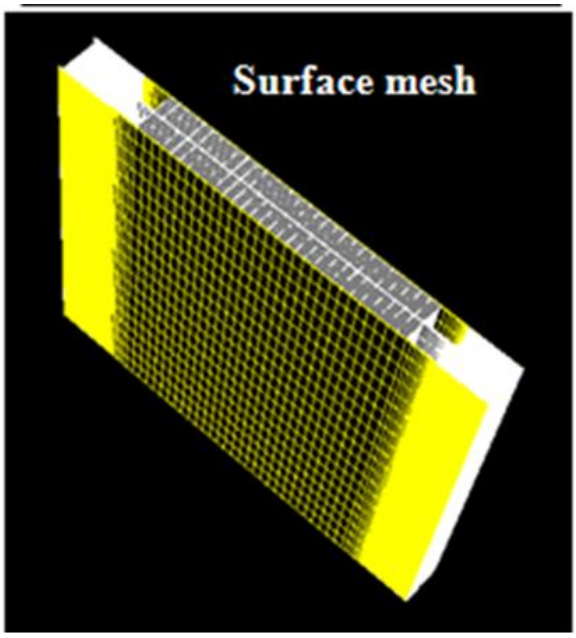

(d). Mesh for the periodic sector

Fig. 4: Computational domain for the fin outside design cooling flow configuration, (a). Top view of the module, (b). Top view of the external fins, (c). Periodic sector, and (d). Mesh for the periodic sector.

RESULTS

A. Pin-fin channel design

Figure 5 shows the average cell temperature (T_{avg}), maximum temperature variation (ΔT) within the cell and air pressure drop. The pressure drop across the channel is only dependent on the flow rate (not the heat generation from the battery since the air properties are assumed constant in the simulation). The pressure drop is 149 Pascal for the flow rate of 200 m^3/h. One of the important cooling parameters is the maximum temperature variation (ΔT) within battery cells. Figure 5 shows that for 500 W and the cooling flow rate of 100 m^3/h show the predicted ΔT is about 0.42 ^0C higher than the requirement of 2 ^0C and for the flow rate of 200 m^3/h, it almost meets the requirement (2.04 ^0C). For 1500 W, the 200 m^3/h flow rate predicts ΔT = 6.11 ^0C which is above the requirement of 5 ^0C and the 600 m^3/h is adequate for the cooling needs.

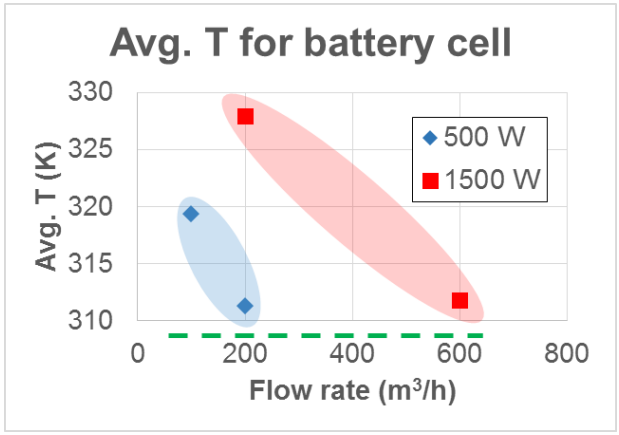

(a). Average cell temperature
Avg. cell temperature limit

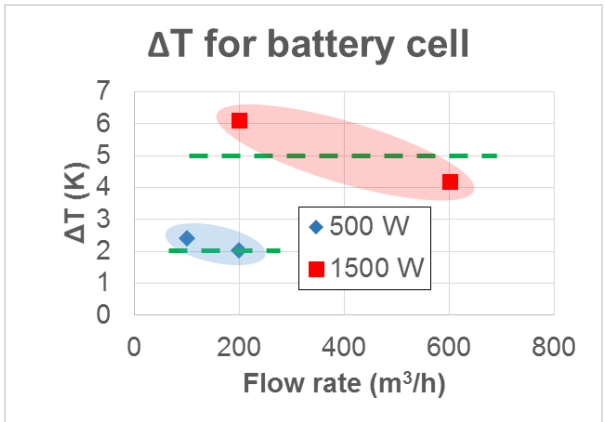

(b). Temperature variation in cell
ΔT limit

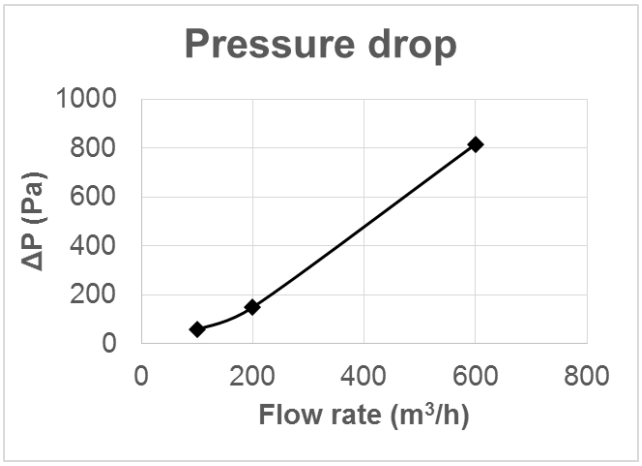

Fig. 5: (a). Average cell temperature (b) temperature variation in battery cell and (c) air pressure drop across air cooling channel for the pin-fin channel case.

The pressure drop relationship can be fitted into a second order polynomial as: $\Delta p = 10.558V^2 + 58.26V$, where V is the average inlet velocity in m/s.

For the current steady state approach, the following relationship holds for the energy balance; $\dot{m}Cp\Delta T = \dot{Q}$, where

$\dot{m} = \rho VA$, the air cooling mass flow rate
Cp = specific heat
$\Delta T = \bar{T}_{exit} - \bar{T}_{in}$, difference between the average inlet and exit air temperatures of the channel
$\dot{Q}$ = total heat generation

This energy balance can be used to check the average air temperature at the exit analytically. The exit temperature can be expressed as $\bar{T}_{exit} = \bar{T}_{in} + \frac{\dot{Q}}{\dot{m}Cp}$.

Table 1 shows the analytical air exit temperatures for all the calculations. The numerical predictions from Fluent are within 0.2% for all cases. The energy balance of the pin fin case shows the general accuracy level of the solution procedure. Although a mesh refinement study might provide more insight in accessing the accuracy and mesh independency of the solution, the present numerical setup and mesh density is fairly adequate to access various cooling concepts with confidence. Also uniform heat generation is assumed in the current study for quick evaluation. In reality, heat generation is highly non-uniform and is more concentrated near the tabs due to high electric current fluxes passing through that narrow area. Both heat generation model of the battery cell and correlation are still to be developed and they are all very cell dependent. The test data weren't quite available for numerical model validation yet during the time of this study.

Table 1 Averaged air temperature at the exit for the pin-fin channel case

Heat Generation (W)	500		1500	
Flow rate (m^3/h)	100	200	200	600
Exit air temp from Fluent	318.51	310.34	326.62	310.18
Exit air temp from analytical solution	318.42	310.71	326.13	310.73
absolute error (%)	0.03%	0.12%	0.15%	0.18%

Figures 6-10 show the results from the 1500 *W* with 600 m^3/h cooling rate. Figure 6 shows the temperature contours for the battery cells. Figure 7 shows the temperature contours only for the bottom portion of the battery cell and the pin-fin. From the temperature contour levels in both figures, it can be seen that near the inlet, the temperatures of the battery cells and the pin-fin are cooled quickly to about 306 ^0K. The cooling air is slowly heated up by the heat dissipated from the battery cells.

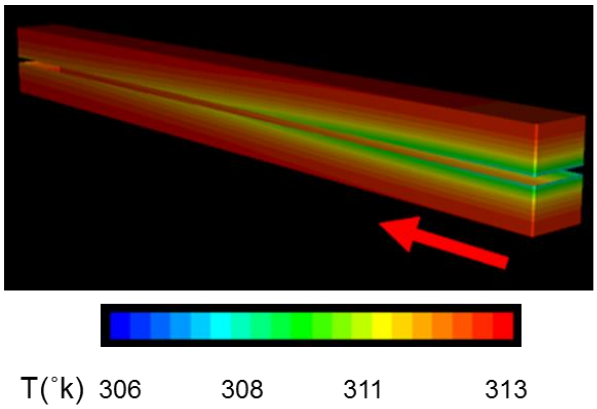

Fig. 6: Temperature contours for the battery cells; 1500 *W* and 600 m^3/h for the pin-fin channel case.

Figure 8 shows the flow velocity vectors (colored by temperature) along a horizontal plane (parallel to the battery cell face). The flow feature is dominated by the separation bubbles behind each pin-fin. The close-up view of the velocity vectors near the inlet and the exit clearly reveals the flow pattern and the streamlines.

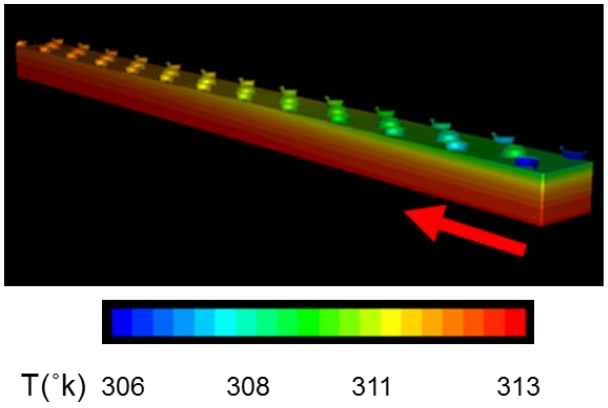

Fig. 7: Temperature contours for the lower battery cell and pin-fins; 1500 *W* and 600 m^3/h for the pin-fin channel case.

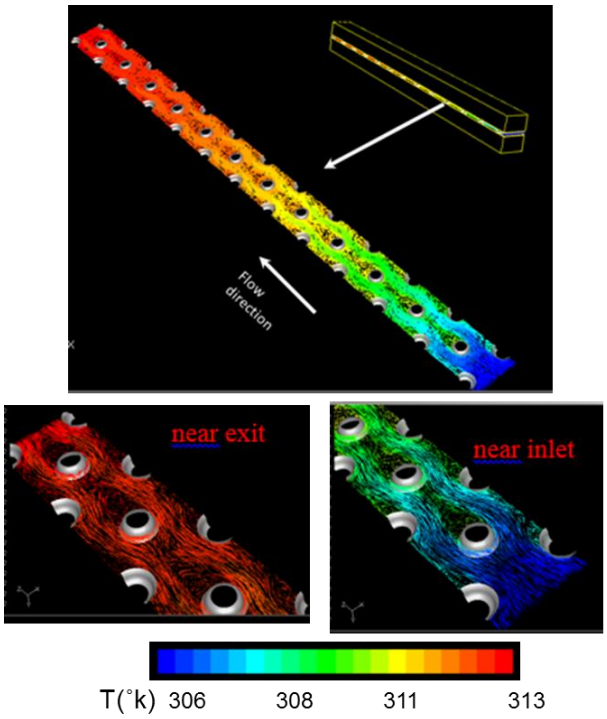

Fig. 8: Air velocity vectors colored by temperature at the mid-plane between upper and lower battery cells; 1500 *W* and 600 m^3/h for the pin-fin channel case.

The temperature distributions along the flow direction at two locations (of the battery cell) are shown in Fig. 9. The temperature at the symmetry plane (blue line) of the cell uppermost surface remains high and more uniform since it is farther away from the cooling air and the temperature variation is within 0.5 ^0K. The other line (red line) in Fig. 9 is at 0.2 *mm* away from the surface. The cooling air flow has strong effects for this temperature distribution. The temperature variation is about 3 ^0K from the inlet to the exit. The air pressure distribution along the centerline of the channel is plotted in Fig. 10. For a fully developed laminar channel flow, the pressure drop is linear which is captured in Fig. 10.

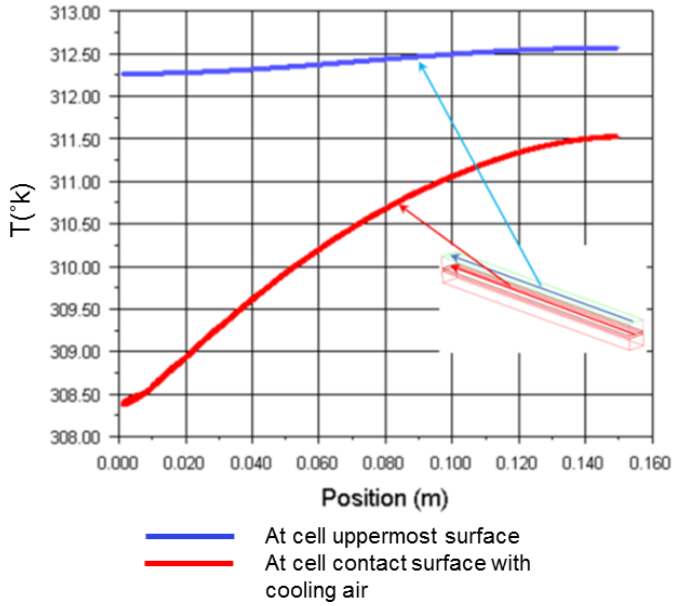

Fig. 9: Temperature distribution for the battery cell from inlet to exit; blue curve: 6.8 *mm* position above the air contact (symmetry plane of the cell), red curve: 0.2 *mm* above the air contact; 1500 *W* and 600 *m³/h* for the pin-fin channel case.

However, due to the presence of the pin-fins on the centerline, the pressure distribution shows local pressure rises and drops in front of and behind the pin-fins. The broken segments in the plot are the locations occupied by the space inside the pin-fins.

Fig. 10: The air pressure distribution along the centerline of the

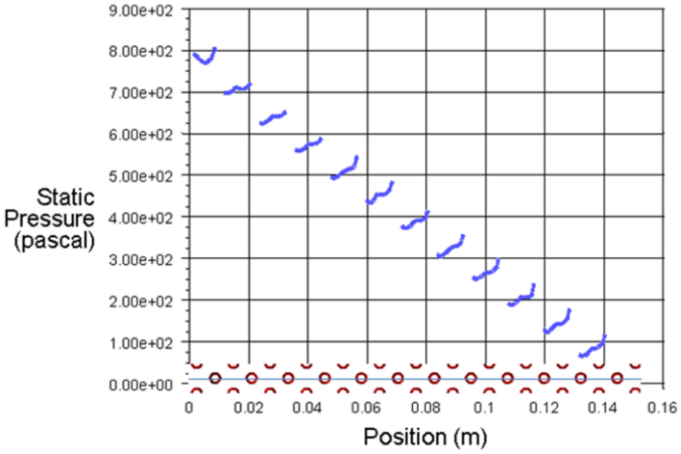

air domain - the broken space indicates the pin-fin location as seen in the insert picture; 1500 *W* and 600 *m³/h*.

B. Fin outside design

For the fin outside design cooling configuration described above, the cooling of the battery occurs in two steps: (1) the battery heat generation is removed by a high conductive thin plate sandwiched between two battery cells and, (2) external convective air is used to remove the heat from the high conductive thin plate through the fins attached to the plate. First, the effect of the cooling flow direction is investigated. In the co-flow configuration the cooling air from both sides of the fins enters and exits from the same direction. The counter-flow configuration is that the cooling air from both sides of the fins enters and exits from the opposite direction. Figure 11 shows the temperature contours for the battery cells including the cooling plate and fins for the co-flow and counter-flow configurations at 1500 *W* and 200 *m³/h*. The effect of the flow directions can be seen very clearly by the contours. Figure 12 shows more detailed comparisons for the battery cell temperatures only (not including the fins and cooling plate) at two heat generations and two cooling flow rates of 100 and 200 *m³/h*, respectively.

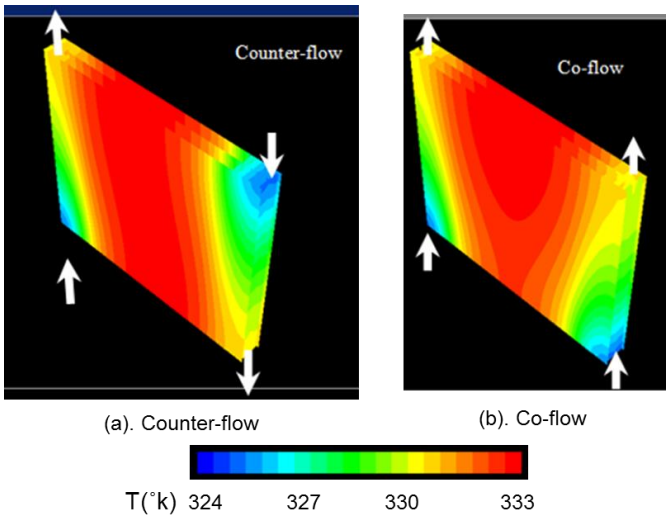

Fig. 11: Temperature contours for battery cells including cooling fins; 1500 *W* and 200 *m³/h* for the fin outside design concept, (a). Counter-flow configuration and (b). Co-flow configuration.

The cooling flow direction, from the results shown in Fig. 12, does not have much impact on the three temperature quantities (average, maximum, minimum) of the battery cells at all. The differences between co-flow and counter-flow configurations are less than 0.2 ^{0}K. The pressure drop for the co-flow (indirect cooling) configuration is shown in Fig. 13. As expected, the pressure drop for the indirect case is very small compared with the direct cooling flow configuration. The pressure drop results for the counter-flow are similar to the co-flow results. One aspect of the indirect cooling is that it produces much smaller ΔT (< 1 ^{0}K for 500 W and < 3 ^{0}K for 1500 W) within the battery cells than the direct cooling for all cooling flow rates. However, the absolute cell temperatures predicted from the indirect cooling for all cooling configurations remain higher than the direct cooling.

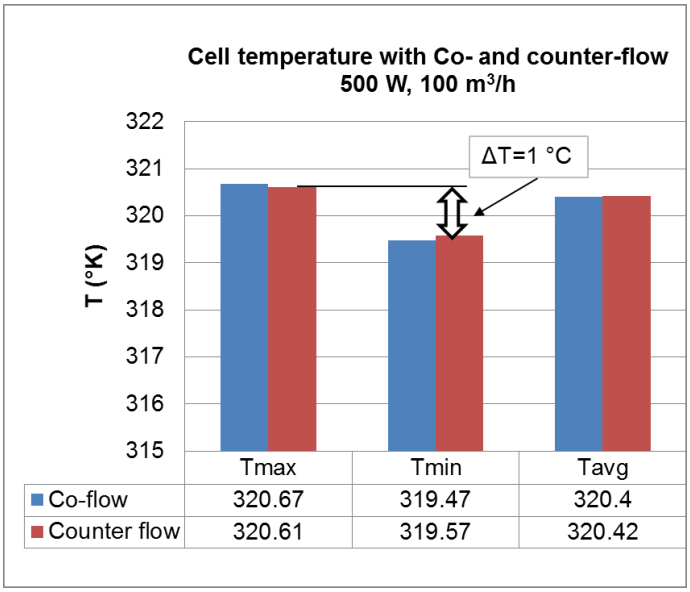

(a). Cell temperature for co- and counter flow with 500 W 100 m³/h.

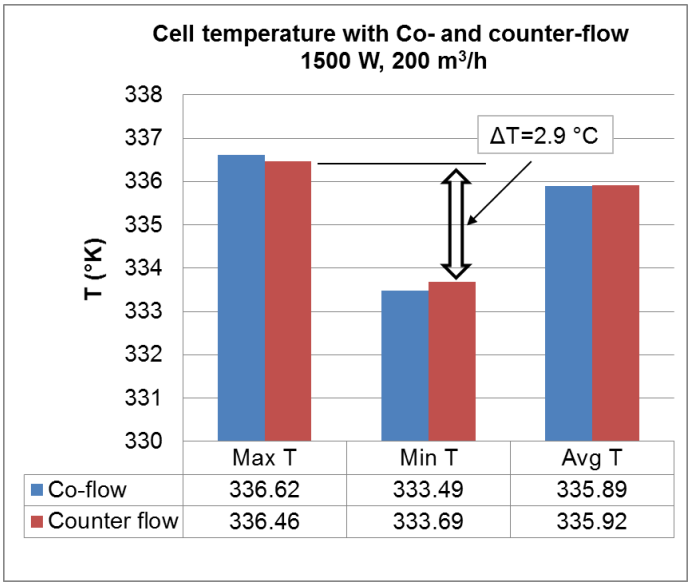

(b). Cell temperature for co- and counter flow with 1500 W 200 m³/h.

Fig. 12: Comparison between maximum, minimum and averaged temperature for the battery cell for co- and counter-flow configurations: upper chart for 500 *W* and 100 *m³/h*, lower chart for 1500 *W* and 200 *m³/*h for the fin outside design concept.

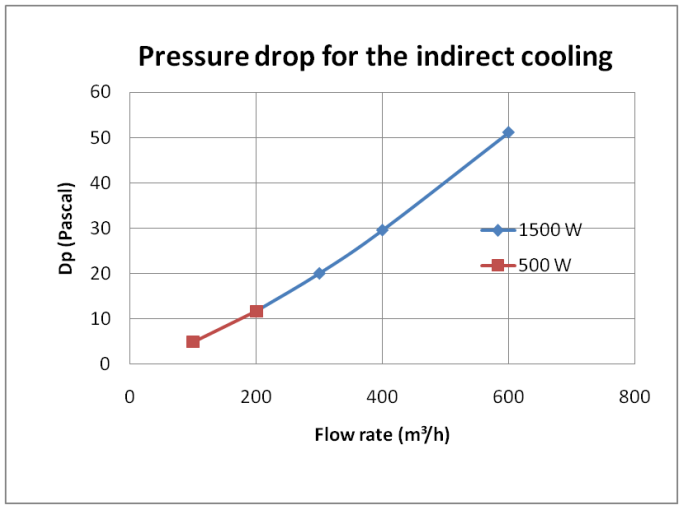

Fig. 13: The Pressure drop for the fin outside design concept.

C. Sensitivity of the thermal conductivity of the cooling plate and fin

To study the effect of the thermal conductivity of the cooling plate material on the battery cell temperature, a series of numerical simulations were performed for thermal conductivities ranging from 202 to 5000 *W/(m ^{0}K)* for heat load of 1500 *W* and 200 *m³/h* flow rate. The results are shown in Figs. 14 and 15.

Figure 14 shows the temperature contours of the battery cells for thermal conductivities of 202, 350, 500, 2000 and 5000 *W/(m ^{0}K)*. The temperature distribution of the battery cells becomes more and more uniform as the thermal conductivity increases. Figure 15 shows detailed cell temperature data as a function of the thermal conductivity. The battery temperatures including the average, maximum, minimum and the ΔT (T_{max}-T_{min}) improve significantly from *K*=202 to *K*=500. As *K* increases from 500 to 2000, the improvement becomes less and the improvement is insignificant for *K* beyond 2000. It should be noted that currently it is possible to use materials with thermal conductivity as high as 1200 *W/(m ^{0}K)* commercially.

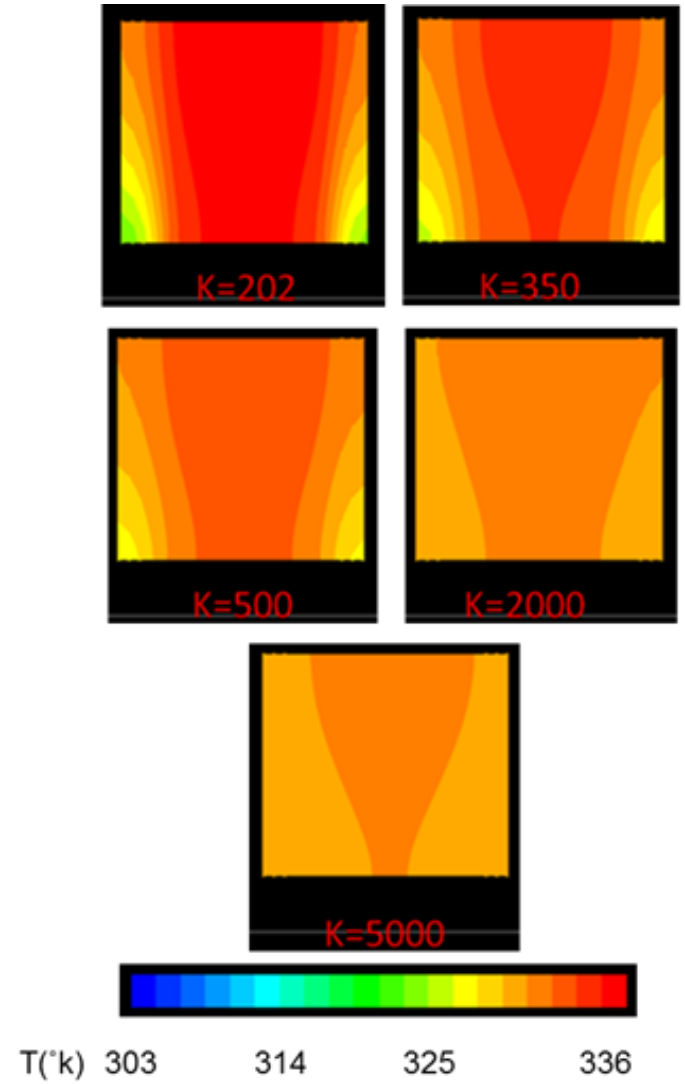

Fig. 14: Battery cell temperature contours for various cooling plate thermal conductivities; 1500 *W* and 200 *m³/h* for the fin outside design concept.

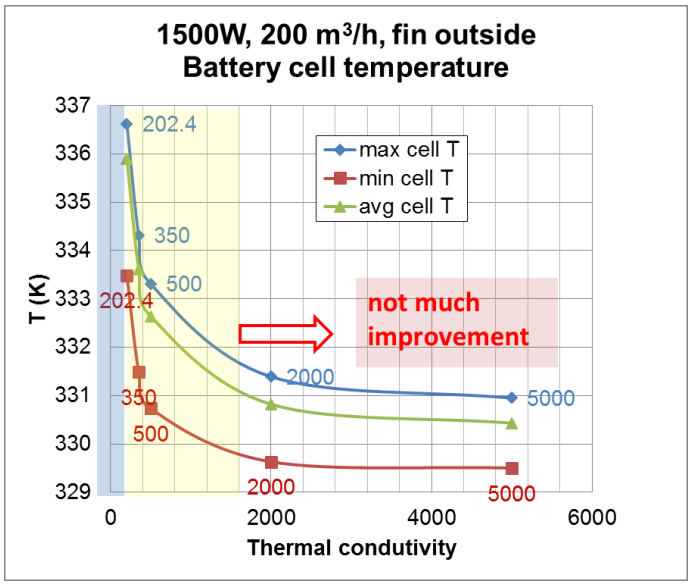

(a). Battery cell temperature

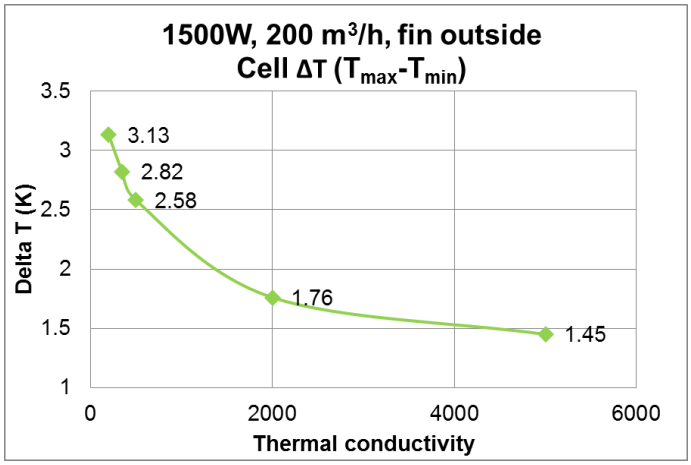

(b). Cell ΔT

Fig. 15: Battery cell temperature and variations with thermal conductivity of the cooling plate; (a) cell temperature for 1500 *W* and 200 *m³/h*, (b) *ΔT* for the 1500 *W* and 200 *m³/h* for the fin outside design concept.

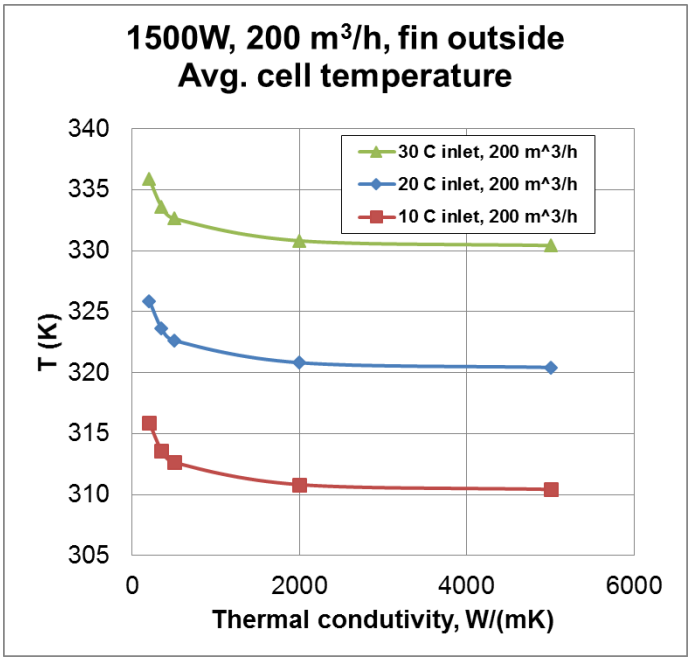

(a). Battery average cell temperature

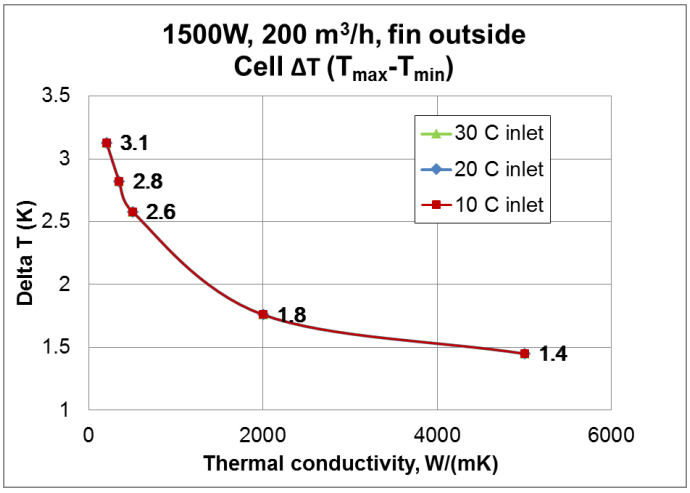

(b). Cell ΔT with thermal conductivity

Fig. 16: (a.) Battery average cell temperature and (b). Cell temperature ΔT (T_{max}-T_{min}) with various thermal conductivities for three air inlet temperatures for the fin outside design cooling.

D. Effect of the air inlet temperature

The air inlet temperature is specified ranging from 10 ^{o}C (283 ^{o}K) to 30 ^{o}C (303 ^{o}K) to understand its influence on the cell temperature. Figure 16 shows the results for the case of 1500 W and 200 m³/h. As can be seen from Fig. 16 (a), the average cell absolute temperature is reduced with the exact amount of the temperature drop (10 ^{o}C drop in each curve) in the air inlet temperature. This is because, for steady state, in order to maintain the same heat dissipation taken away from the battery cell, the heat fluxes (and the temperature gradients) in the cooling plate, fin and cell are the same for all air inlet temperatures. Thus, the same temperature drops in the cooling plate, fin and cell are in direct response of the same temperature gradient. With the same reason, the cell ΔT (T_{max}-T_{min}) shown in Fig. 16 (b) is unchanged and unaffected by different air inlet temperatures since the cell absolute temperatures are shifting down by the same amount of changes in the inlet air temperatures.

CONCLUSIONS

In this paper, three-dimensional CFD models were used to study detailed cell-level thermal and pressure drop performance of air cooling concept for the battery pack concepts: "the pin-fin channel design" and "the fin outside design" cooling configurations. In the pin-fin channel design cooling concept, the cooling air is in direct contact with the battery cell surfaces by introducing the cooling air from manifold into the cooling channels between battery cells.

For the fin outside design cooling concept, the cooling air is not in direct contact with the battery cell surfaces; rather, a metal cooling plate with fin structures is placed between the battery cells with no air flowing between the cells.

The following summary is drawn from this study:

1. For the pin-fin channel concept, all specified flow rates predict higher averaged cell temperatures than the required 308 ^{o}K. For cell temperature variation, ΔT, the higher flow rates (200 m^3/h for 500 W and 600 m^3/h for 1500 W) meet the cell temperature distribution (ΔT) requirement (< 2 ^{o}C *for* 500 W *and* < 5 ^{o}C for 1500 W). The low flow rates, i.e., 100 m^3/h for 500 W and 200 m^3/h for 1500 W, lack the necessary cooling capacity to meet the thermal requirements.
2. For the fin outside design concept, the numerical predictions show that the cell temperature ΔT's for all flow configurations satisfy the requirement (< 2 ^{o}C for 500 W and < 5 ^{o}C for 1500 W).
3. The numerical predictions for the fin outside design concept indicate that the absolute temperatures are all higher than the thermal requirement (< 35 ^{o}C or < 308 ^{o}K) with the 303 ^{o}K air inlet temperature. The absolute cell temperatures for the fin outside design cooling depend strongly on the performance of the outside fin cooling capacity and/or the air inlet temperature. In order to meet the absolute cell temperature requirement, one has to lower the inlet air temperature or improve the outside fin design to enhance the heat transfer.

4. The fin outside design concept generates a lower pressure drop than the pin-fin cooling concepts for all cases.
5. For the fin outside design concept, using high thermal conductivity material (such as copper or material coatings) for the cooling plate can reduce the cell temperature and also improves the cell temperature uniformity (K ranging from 202 to 500 *W/(m ^{o}K)*. This effect diminishes for *K* values above 2000 *W/(m ^{o}K)*.

NOMENCLATURE

EREV	Extended Range Electric Vehicle
EV	Electric Vehicle
PHEV	Plugin Electric Vehicle
ρ	Density, *Kg/m³:*
Cp	Specific heat, *J/(kg ^{o}K)*
K	Thermal conductivity, *W/(m ^{o}K)*
μ	Dynamic viscosity, *Kg/(m s)*
$\dot{Q}$	Total heat generation, *W*
V	Air velocity, *m/s*
A	Channel cross section area, m^2
$\dot{m} = \rho VA$	Mass flow rate, *Kg/s*
ΔT	Temperature difference, ^{o}K
Δp	Pressure difference, *Pa*
T_{max}	Maximum cell temperature, ^{o}K
T_{min}	Minimum cell temperature, ^{o}K
T_{avg}	Average cell temperature, ^{o}K
T_{in}	Air inlet temperature, ^{o}K
T_{exit}	Air exit temperature, ^{o}K

ACKNOWLEDGMENTS

The authors would like to express their gratitude to Stephan Fell, Reiner Essinger, Steffan Böhm and Gordon Anderson at GM's CAE research group at Mainz-Kastel, Germany for their technical discussion and data for this analysis.

REFERENCES

1. Payne, J. Niedzwiecki, M, Ketkar, S. and Isayev I., "Thermal Characterization & Management of PHEV Battery Packs", SAE 2009-01-3069, 2009.
2. Ghosh D., Maguire, P. and Zhu D., "Design and CFD Simulation of a Battery Module for a Hybrid Electric Vehicle Battery Pack", SAE 2009-01-1386, 2009.
3. Kim U., Ryu, C., Shin C., Han T., and Park S., "A Study on the Thermal Behavior of a Lithium-ion Battery during Charging," 15th International meeting on Lithium Batteries, Montreal, Canada, 2010.
4. Mohammadian, S. K. and Zhang Y., "Thermal management optimization of an air-cooled Li-ion battery module using pin-fin heat sinks for hybrid electric vehicles", pp. 431-439, Vol. 273, J. of Power Sources, 2015.
5. Zhang, X., Kong X., Li, G. and Li, J., "Thermodynamic assessment of active cooling/heating methods for lithium-ion batteries of electric vehicles in extreme conditions", pp. 1902-1101, Vol., 64, Energy, 2014.
6. Fluent 6.3.37, ANSYS, 2009.
7. Private communication with LGChem.